Acta Crystallographica Section A
Foundations of Crystallography
ISSN 0108-7673

Received 28 February 2003
Accepted 24 October 2003

Electron localization functions obtained from X-ray constrained Hartree–Fock wavefunctions for molecular crystals of ammonia, urea and alloxan[1]

Dylan Jayatilaka* and Daniel Grimwood

Chemistry, School of Biomedical and Chemical Sciences, University of Western Australia, Crawley 6009, Australia. Correspondence e-mail: dylan@theochem.uwa.edu.au

Constrained Hartree–Fock wavefunctions in the superposition of isolated molecules model have been calculated from precise X-ray diffraction data on crystals of ammonia (NH_3), urea [$CO(NH_2)_2$] and alloxan [$(CO)_4(NH)_2$]. The X-ray constrained wavefunctions have been used to derive and examine 'electron localization' information, quantified by the true and approximate electron localization function (ELF), and the true and approximate Fermi hole mobility function (FHMF). The plots of the Fermi hole mobility function are the first to appear in the literature. The results are compared with corresponding isolated-molecule Hartree–Fock calculations to gauge the effect of the crystal environment on the isolated molecules. An error analysis is performed to indicate the features in the plots which are well determined from the experimental data. The results from all plots are broadly consistent, but the approximate ELF shows some artifacts relative to the true ELF.

1. Introduction

This paper is concerned with the extraction of chemically useful information from the one-particle reduced electron density matrix – specifically, electron localization function information from orbitals and density matrices obtained from Hartree–Fock wavefunction calculations, and such Hartree–Fock wavefunction calculations that have been constrained to reproduce the results of precise X-ray diffraction experiments.

In some important work on the topic of extracting chemical information from electronic-density matrices, Luken and co-workers (Luken, 1982; Luken & Beratan, 1982; Luken & Culberson, 1982, 1984; Luken, 1990) have reiterated (Bader & Stephens, 1975; Silvi & Savin, 1994) the significance of the Fermi hole. The Fermi hole is simply the function representing the depression in the probability of detecting an electron around the position of a probe electron, as the position of the probe electron is moved around the molecule. Luken and co-workers proposed the use of the relative Fermi hole mobility function (FHMF) as a means of detecting regions in a molecule where electron pairs are localized. For a single closed-shell determinant wavefunction made from orbitals $\phi_i(\mathbf{r})$ and with density $\rho(\mathbf{r})$, it is given by

$$\mathrm{FHMF}(\mathbf{r}) = \left(\frac{2}{\rho^2}\right)\sum_{\nu=1}^{3}\sum_{i>j}\left[\phi_i\frac{\partial\phi_j}{\partial r_\nu} - \phi_j\frac{\partial\phi_i}{\partial r_\nu}\right] - \left(\frac{2}{\rho}\right)\sum_{i,j}\phi_i\phi_j T_{ij}, \tag{1}$$

where $T_{ij} = \langle\phi_i| - (1/2)\nabla^2|\phi_j\rangle$ are kinetic energy integrals over orbitals ϕ_i and ϕ_j (atomic units are used here and throughout the paper). In principle, the FHMF can be calculated for more complicated wavefunctions, but currently there are no closed-form formulae available. The mobility function is interesting because it has the dimensions of energy, and arguments can be given that support the interpretation that depressions in the FHMF represent regions where electron pairs are localized, while the paths between depressions are associated with the energy to transfer an electron from one localized region to another (relative to an ideal conductor) (Luken, 1990). That is, the function can be interpreted as a three-dimensional potential-energy surface for electron transfer. Unfortunately, plots of FHMF($\mathbf{r}$) have never been made: instead, what is usually plotted is an approximation to this, where the last term in equation (1) is replaced by the value it takes in a free-electron gas. This yields the approximate relative Fermi hole mobility function,

$$\mathrm{AFHMF}(\mathbf{r}) = \left(\frac{2}{\rho^2}\right)\sum_{\nu=1}^{3}\sum_{i>j}\left[\phi_i\frac{\partial\phi_j}{\partial r_\nu} - \phi_j\frac{\partial\phi_i}{\partial r_\nu}\right] - (3\pi/4)(\rho/2)^{2/3}. \tag{2}$$

Later, Becke & Edgecombe (1990) and others (Savin *et al.*, 1991; Silvi & Savin, 1994) used arguments based on the spherical average of the conditional pair probability function around the position of a reference electron, or the kinetic energy density, to suggest the electron localization function (ELF) as a means of understanding and quantifying electron

[1] Work presented at the Microsymposium on Quantum Crystallography, XIX IUCr Congress, Geneva, Switzerland, August 2002.

pairing information. For a closed-shell determinant wavefunction as before, the ELF is defined by

$$\mathrm{ELF}(\mathbf{r}) = [1 + (D_P/D_0)^2]^{-1}, \quad (3)$$

where D_P is the Pauli kinetic energy and D_0 is the kinetic energy of a free-electron gas with density locally equal to $\rho(\mathbf{r})$, respectively,

$$D_P(\mathbf{r}) = (1/2)\sum_i |\nabla\phi_i|^2 - (1/8)|\nabla\rho|^2/\rho, \quad (4)$$

$$D_0(\mathbf{r}) = (3/10)(3\pi^2)^{2/3}\rho^{5/3}. \quad (5)$$

The ELF involves terms very similar to the FHMF. The main difference is that one uses a ratio relative to a free-electron gas reference value, as opposed to a difference, to establish the location of electron pairs. There are now numerous examples of the utility of the ELF for interpretive chemical studies [see, for example, Savin *et al.* (1991), Silvi & Savin (1994) or Kohout *et al.* (2002); a comprehensive bibliography can be found at Frank Wagner's ELF home page, http://www.cpfs.mpg.de/ELF/index.html].

Note that the localization functions described above may only be calculated from a knowledge of the density matrix. Ideally, it would be desirable to obtain electron localization function information directly from an experimental density matrix. However, to date it has been difficult to obtain true experimental measurements of the density matrix. Nevertheless, the desire to access the information in the localization functions has led some to suggest their calculation using approximations based on the density only. Thus, for example, Tsirelson & Stash (2002) argue the case for using the Kirzhnits approximation for the kinetic energy, the first term in (4), to obtain an approximate ELF

$$\mathrm{AELF}(\mathbf{r}) = [1 + (D_{P,\mathrm{DFT}}/D_0)^2]^{-1}, \quad (6)$$

where

$$D_{P,\mathrm{DFT}}(\mathbf{r}) = (3/10)(3\pi^2)^{2/3}\rho^{5/3} - (1/9)|\nabla\rho|^2/\rho + (1/6)\nabla^2\rho. \quad (7)$$

These workers have produced plots of the AELF in real space for a number of systems, using electron densities ρ obtained from X-ray diffraction experiments using the Coppens–Hansen 'multipole approximation'.

Recently, it has become fairly easy to obtain constrained Hartree–Fock (CHF) wavefunctions from precise X-ray diffraction data on molecular crystals (Jayatilaka, 1998; Jayatilaka & Grimwood, 2001; Grimwood & Jayatilaka, 2001; Bytheway *et al.*, 2002). The wavefunctions are, essentially, the experimental Hartree–Fock–Kohn–Sham wavefunctions of density functional theory (Hohenberg & Kohn, 1964). While the density matrices from such experimentally constrained wavefunctions do not constitute a true measurement, they do include in some sense the effects of the X-ray measurements. These effects are primarily those due to the crystal lattice and the effects due to electron correlation. Parr and co-workers make the bold statement that such Kohn–Sham wavefunctions provide a solution to the problem of obtaining wavefunctions from experimental data (Zhao & Parr, 1993; Zhao *et al.*, 1994). However, it must be emphasized that there are indications that, for some systems, the density matrix can only be properly reconstructed by combining real-space charge-density information (as obtained from, *e.g.*, X-ray scattering data) *and* momentum-space charge-density data (obtained from, *e.g.*, Compton profile scattering experiments) (Schmider *et al.*, 1992).

Given that X-ray constrained Hartree–Fock wavefunctions (and the corresponding density matrices) are available, the interesting question arises as to what chemical information, specifically electron localization information, is contained in them that is not contained in the density itself; and how these effects compare when density-only approximations are used for the electron localization functions, as described above.

In the rest of the paper, our intention is firstly to present plots of the electron localization functions above, for wavefunctions that have been constrained to reproduce the results of X-ray experiments. We pay particular attention to (i) the Fermi hole mobility function FHMF($\mathbf{r}$), which is exhibited for the first time, and (ii) a comparison of the localization function plots with the approximate ELF, AELF($\mathbf{r}$), which is based solely on the density.

2. Electron localization information obtained from Hartree–Fock, and X-ray constrained Hartree–Fock wavefunctions

2.1. Details of calculations

The details of the experimental data, the calculation of the X-ray constrained Hartree–Fock wavefunctions and methods used to estimate the errors in the plots were described in Grimwood *et al.* (2003), but are reproduced here to aid the reader.

For urea, structure-factor data were taken from Swaminathan, Craven, Spackman & Stewart (1984), who used neutron scattering data to determine the atomic positions and atomic displacement parameters (ADP's) (Swaminathan, Craven & McMullan, 1984). The final χ^2 obtained from the constrained fitting procedure was 1.9. For alloxan, X-ray structure factors, ADP's, and neutron positional data were taken from Swaminathan *et al.* (1985). Note that in the previous publication (Grimwood *et al.*, 2003) not all structure-factor data were used, as claimed, owing to a data-processing error resulting in only the first three pages of experimental structure factors being used (as retrieved from the IUCr electronic archives). In this paper, all structure factors were used. The final χ^2 obtained from the constrained fitting procedure was 2.3, compared with the isolated-molecule Hartree–Fock χ^2 of 3.4. For ammonia, the experimental unit-cell parameters and structure-factor magnitudes were obtained by Boese *et al.* (1997). Prior to use, the experimental intensities for ammonia were merged and averaged, and corrected for absorption and Lorentz polarization effects (Figgis *et al.*, 1998). After averaging, 84 unique reflections

were obtained for ammonia ($\sin\theta/\lambda < 0.71$ Å^{-1}, $|F_h| > 3\sigma_h$). The final χ^2 obtained from the constrained fitting procedure was 1.0.

The fitting process for ammonia was performed until a χ^2 of 1.0 was reached, since this corresponds to agreement with experiment, on average, of one experimental standard deviation. The fitting process for urea and alloxan was done as far as possible before convergence issues with the self-consistent field (SCF) method prevented a lower χ^2 from being obtained.

A Dunning DZP basis set (Dunning, 1970) was used in all calculations for alloxan and urea reported in this paper. A

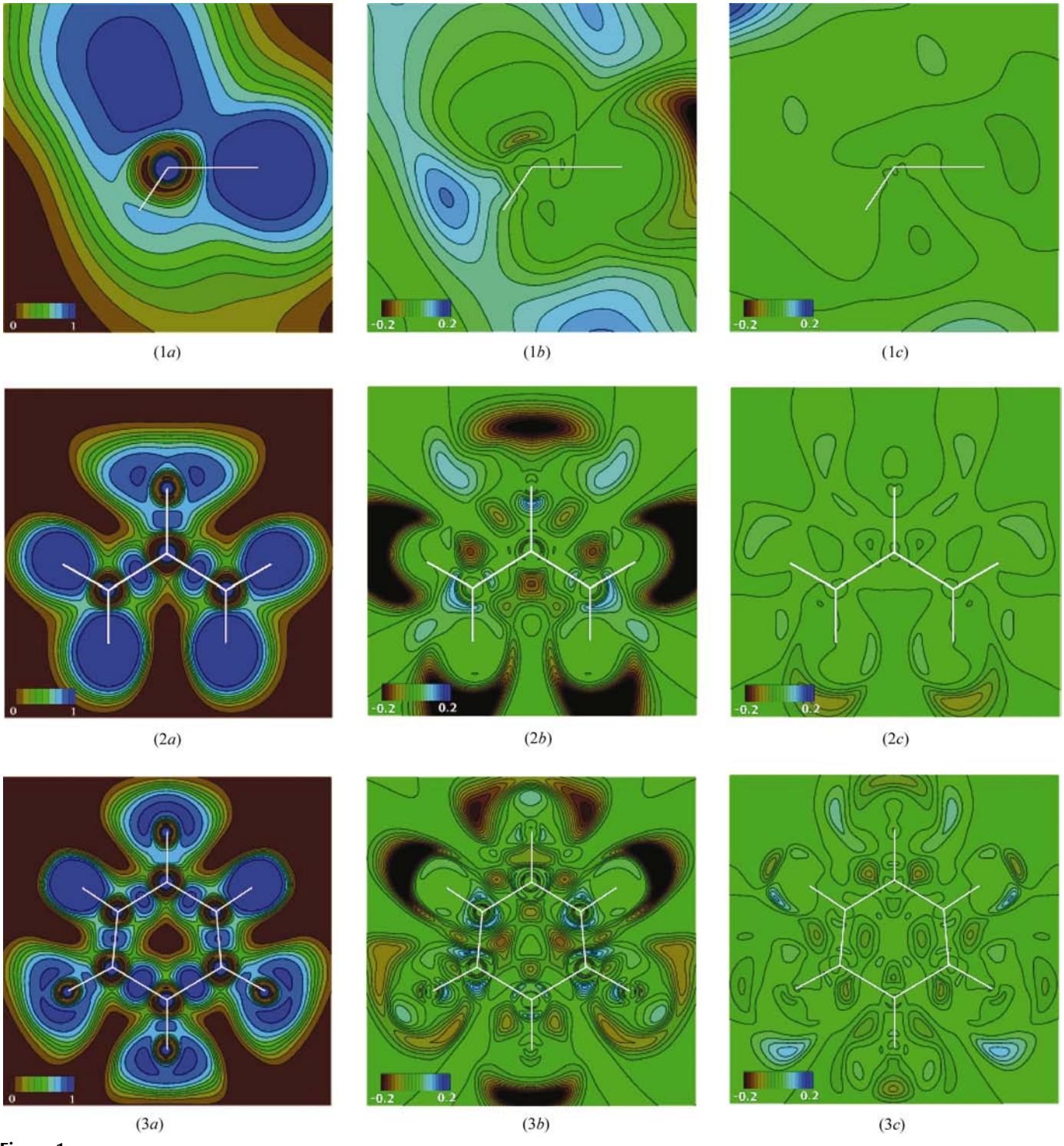

Figure 1
Plots of (*a*) the ELF for the X-ray constrained Hartree–Fock wavefunction (contours at 0.1 increments), (*b*) the difference between the ELF for the constrained wavefunction and the isolated-molecule Hartree–Fock wavefunction (contours at 0.02 increments), and (*c*) the error in the experimentally derived ELF owing to simulated Gaussian noise in the X-ray data (contours at 0.02 increments), for (1) ammonia, (2) urea and (3) alloxan.

previous study on α-oxalic acid dihydrate showed that this basis set was adequate for reproducing constrained Hartree–Fock calculation results obtained using larger triple-ζ basis sets (Grimwood & Jayatilaka, 2001). To be consistent with our earlier paper (Bytheway *et al.*, 2002), a Pople 6-311G++(2*d*,2*p*) basis (Krishnan *et al.*, 1980) was used for all ammonia calculations.

The electron localization function plots that are made refer to the isolated molecules in the crystal, and the perturbation of these isolated molecules by the crystal environment. The

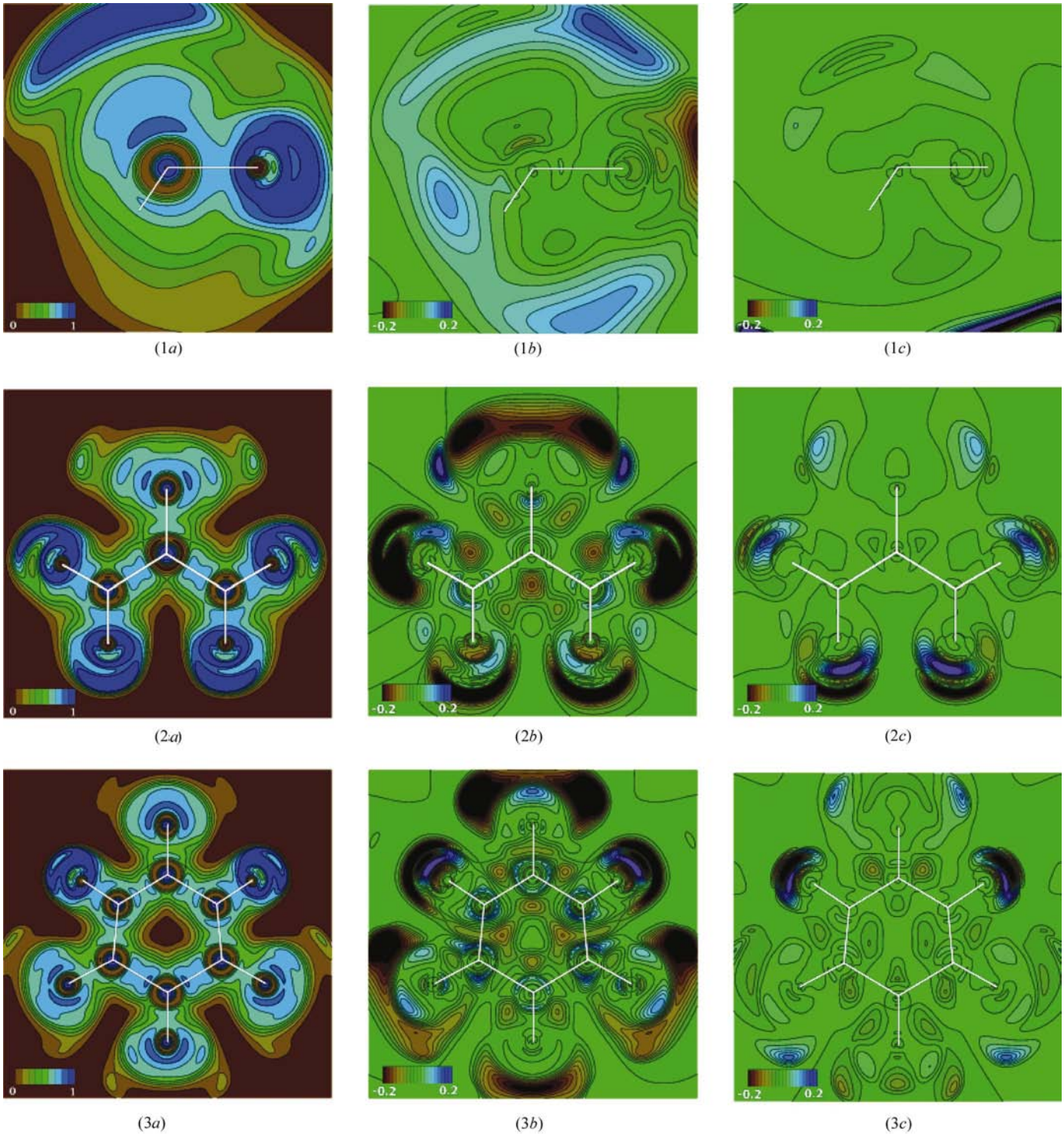

Figure 2
Plots of (*a*) the AELF for the X-ray constrained Hartree–Fock wavefunction (contours at 0.1 increments), (*b*) the difference between the AELF for the constrained wavefunction and the isolated-molecule Hartree–Fock wavefunction (contours at 0.02 increments), and (*c*) the error in the experimentally derived AELF owing to simulated Gaussian noise in the X-ray data (contours at 0.02 increments), for (1) ammonia, (2) urea and (3) alloxan.

effect of neighbouring molecules in the crystal is not displayed.

The error in each electron localization function plot is calculated by adding an infinitesimal amount of Gaussian noise to the experimental data (using the experimental σ values to estimate Gaussian errors in each reflection), and by taking a derivative with respect to this random noise, using a central limit finite difference procedure, at each pixel in the plot. A noise parameter of $\alpha = \pm 0.1$ was used, as described in Grimwood *et al.* (2003).

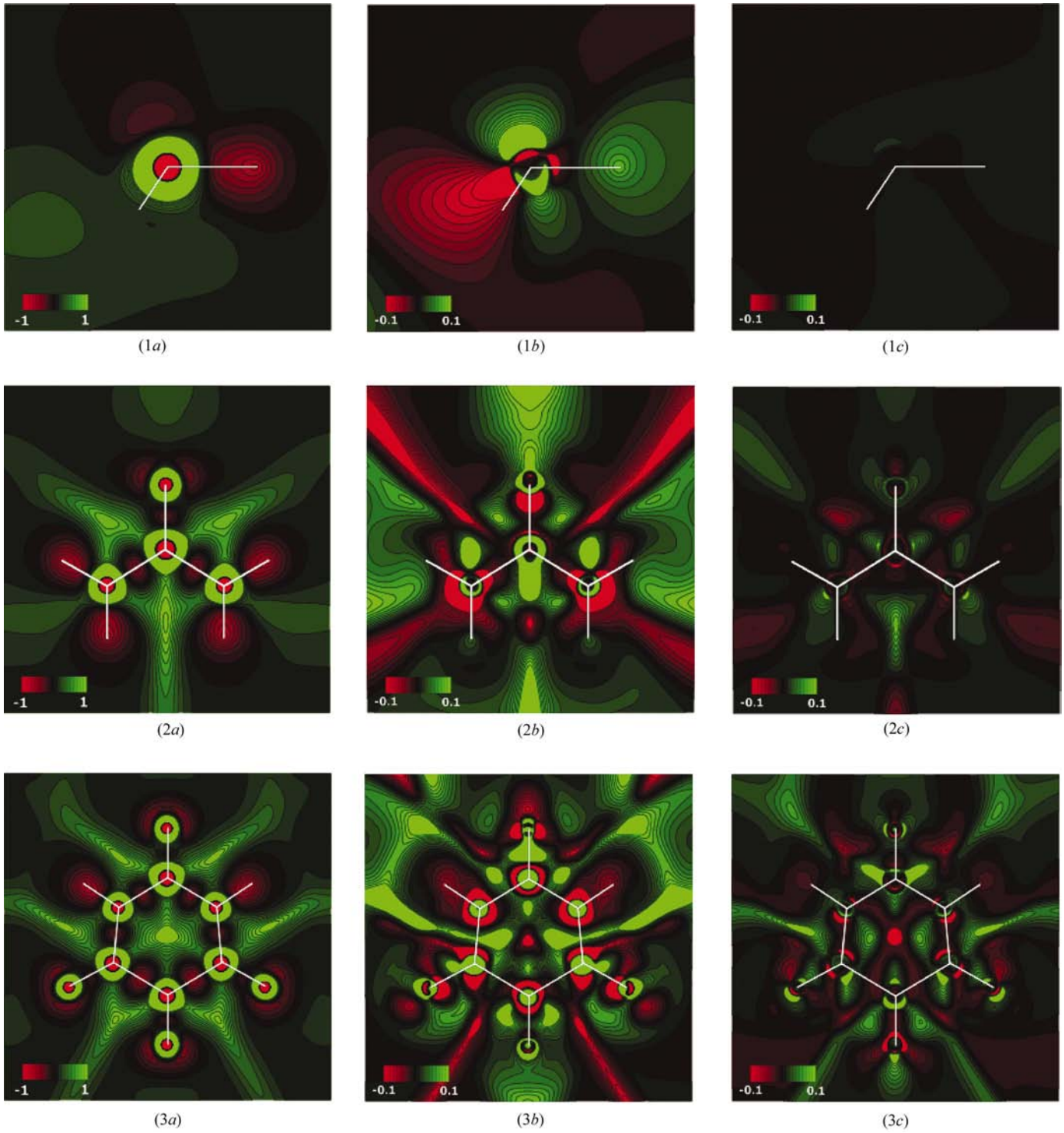

Figure 3
Plots of (*a*) the AFHMF for the X-ray constrained Hartree–Fock wavefunction (contours at 0.1 a.u. increments), (*b*) the difference between the AFHMF for the constrained wavefunction and the isolated-molecule Hartree–Fock wavefunction (contours at 0.02 a.u. increments), and (*c*) the error in the experimentally derived AFHMF owing to simulated Gaussian noise in the X-ray data (contours at 0.01 a.u. increments), for (1) ammonia, (2) urea and (3) alloxan.

2.2. Discussion of the results

Figs. 1–4 are, respectively, plots of the ELF, AELF, AFHMF and FHMF. We have also displayed, for comparison, the Laplacian of the electron density in Fig. 5, because it is often used to display electron shell structure. In each plot, we show (*a*) the electron localization function (*e.g.* ELF or FHMF) for the X-ray constrained Hartree–Fock wavefunction, (*b*) the difference between the experimentally derived electron localization function and the corresponding plot obtained from an

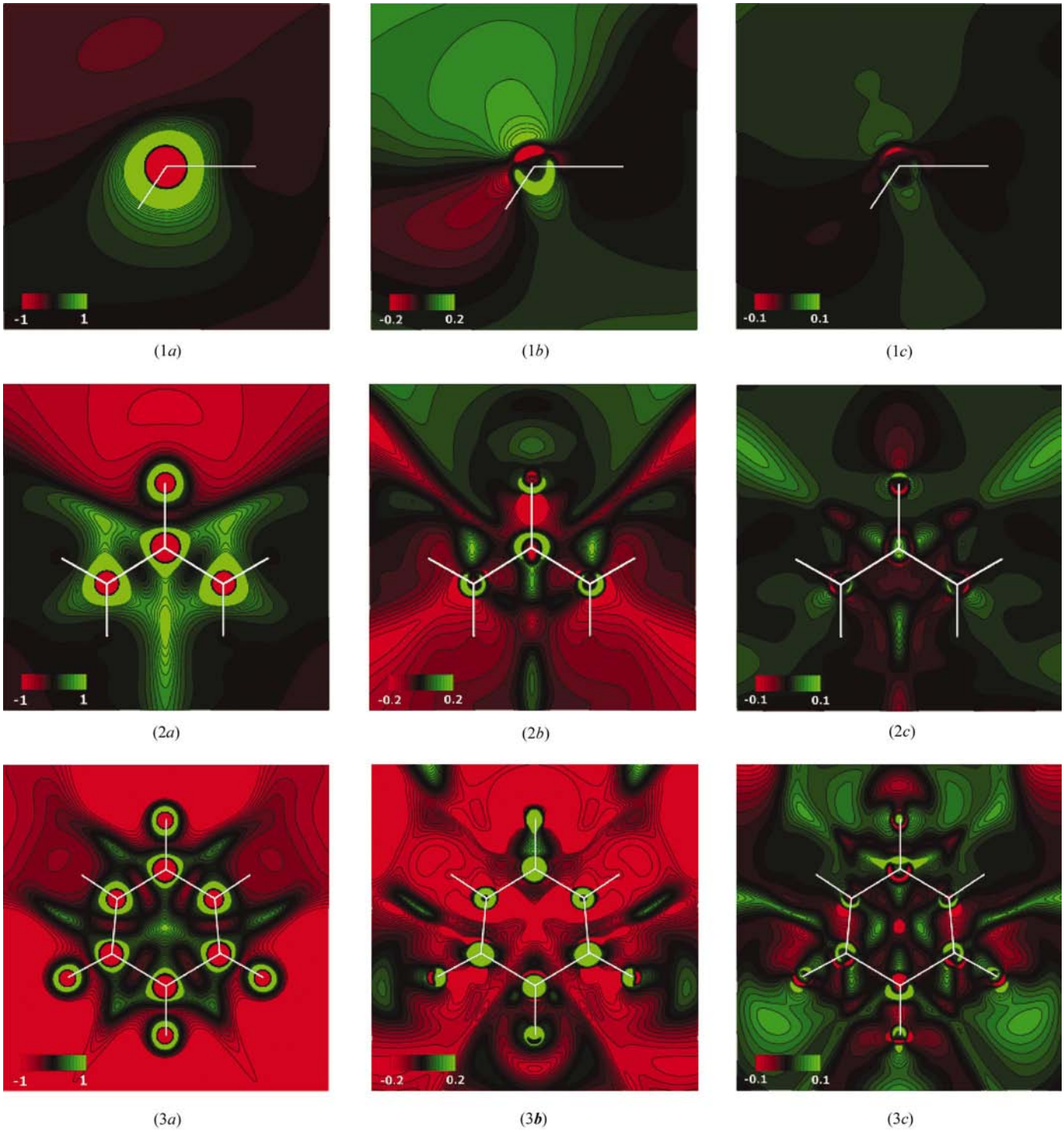

Figure 4
Plots of (*a*) the FHMF for the X-ray constrained Hartree–Fock wavefunction (contours at 0.1 a.u. increments), (*b*) the difference between the FHMF for the constrained wavefunction and the isolated-molecule Hartree–Fock wavefunction (contours at 0.02 increments), and (*c*) the error in the experimentally derived FHMF owing to simulated Gaussian noise in the X-ray data (contours at 0.01 increments), for (1) ammonia, (2) urea and (3) alloxan.

isolated Hartree–Fock wavefunction, and (*c*) the error in the experimental electron localization function owing to Gaussian noise. The plots are shown for (1) ammonia, (2) urea and (3) alloxan. Superposed in white on each figure is the nuclear framework of the molecule, which makes clear the orientation of the plot. Note the varying contour levels, especially for Fig. 4.

All the electron localization function plots are broadly consistent with one another, except in the case of the FHMF, where regions of space corresponding to core, valence and

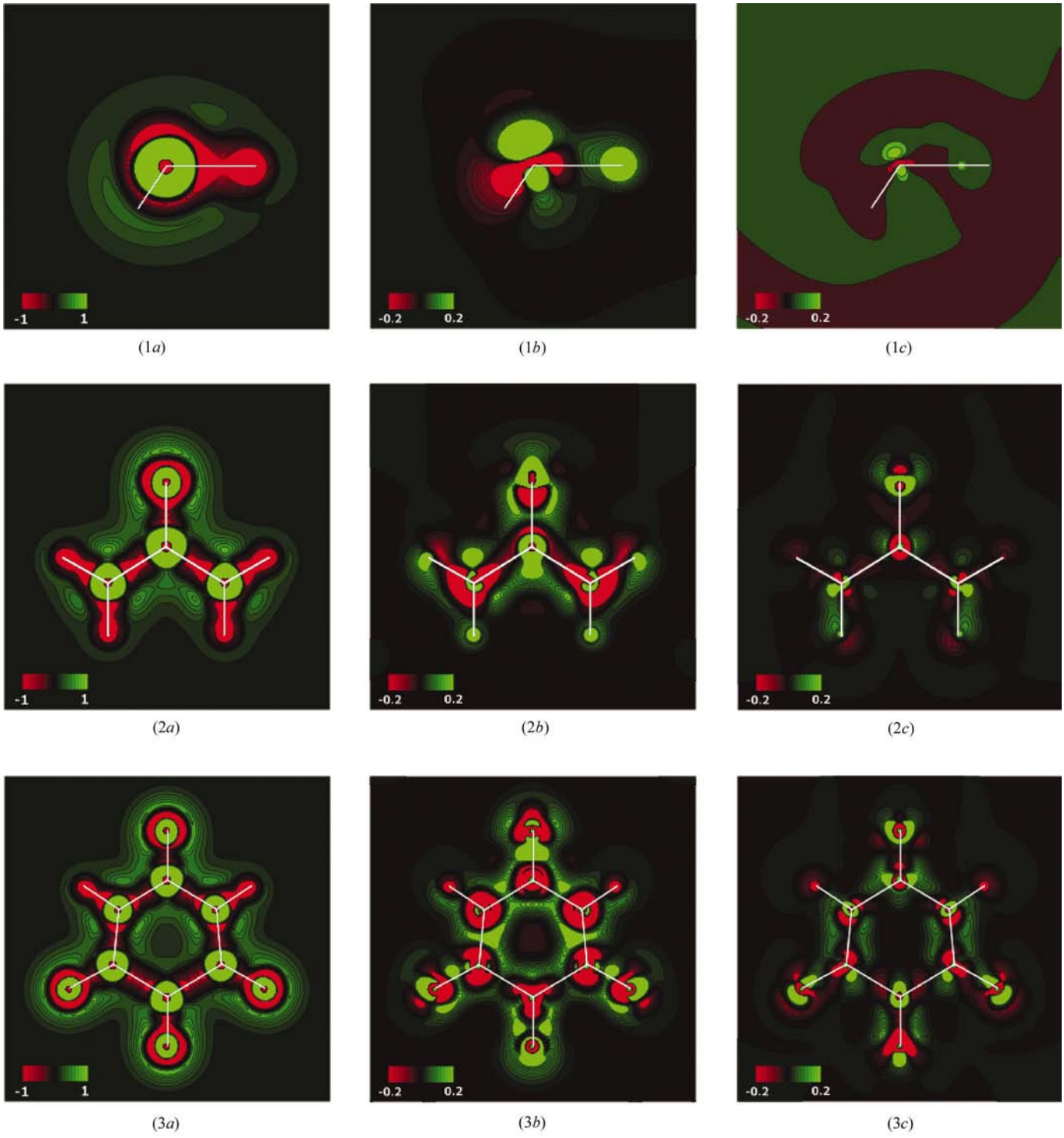

Figure 5
Plots of (*a*) the Laplacian for the X-ray constrained Hartree–Fock wavefunction (contours at 0.1 a.u. increments), (*b*) the difference between the Laplacian for the constrained wavefunction and the isolated-molecule Hartree–Fock wavefunction (contours at 0.02 a.u. increments), and (*c*) the error in the experimentally derived Laplacian owing to simulated Gaussian noise in the X-ray data (contours at 0.02 a.u. increments), for (1) ammonia, (2) urea and (3) alloxan.

lone 'electron pairs' are clearly delineated. In the case of the ELF and the AFHMF, the agreement is very good (keep in mind that the approximate Fermi hole mobility function is on a pseudo-energy scale, so that negative regions loosely correspond to 'electron-pair' regions; whereas for the ELF plots those regions correspond to the values close to 1).

On the other hand, the FHMF does not highlight the lone-pair regions very clearly, nor any core-electron structure around the H atoms: only the core shell structure around heavy atoms is clearly delineated. In addition, the value of the true FHMF does not appear to approach zero at long range, like the AFHMF: at long range, the value can be negative. The FHMF does not involve any reference to the electron gas in its definition, so one can surmise that the use of the electron gas as a kind of reference point is very important in highlighting the regions where electron pairs are assumed to be. However, the electron gas reference is not necessary, since the Laplacian of the electron density is able to distinguish regions of charge concentration that usually correspond to the notion of an electron-pair and shell structure (Bader, 1990), as is seen in the final figure. (Note, however, that the lone-pair structure in ammonia and urea is not displayed at all by the Laplacian.)

A closer analysis shows that it is the last term in equation (1) that is responsible for the long-range behaviour of the FHMF. Clearly, the numerator (comprised of kinetic energy integrals) must become a significant proportion of the total density ρ (in the denominator) at long range. It seems unlikely that this effect is an artifact of the use of Gaussian basis functions in the X-ray constrained Hartree–Fock wavefunction. In fact, we observe that negative values occur in basins close to the O atoms, indicating that a probe electron would be relatively stable in these regions; a conclusion that is fairly intuitive and supports the pseudo-energy interpretation of the FHMF already mentioned. We note however that the variation in scale of the FHMF makes it more difficult to compare between different species. It appears that the pseudo-energy interpretation of the FHMF does not coincide completely with the chemists' notion of electron-pair localization.

Although there is broad agreement between ELF, AELF and AFHMF, there are clear differences. The AELF has very marked and unusually clear shell structure around H atoms compared with its ELF counterpart. Also, the atom–atom bond regions appear to be 'split', contrary to expectation, although similar to the Laplacian. The lone-electron pair regions also appear to be much contracted relative to the ELF. The former split-bond feature can already be seen in plots by Tsirelson & Stash (2002) for urea and was pointed out by them. It seems to us that the strong H-atom shell structure and the bond-splitting anomalies combine in the case of urea to generate a very unusual region, also seen by Tsirelson & Stash (2002), and identified by them as hydrogen bonding with a 'lock-and-key' type interaction. Given that the corresponding features are absent in the ELF plot, we conclude that these are artifacts of the Kirzhnits approximation, and therefore without physical significance. This is a conclusion noted by Tsirelson & Stash (2002) who note also that Yang *et al.* (1986) expect unphysical negative regions near atomic cores owing to the gradient expansion of the kinetic energy. In addition, a comparison with the error in the AELF plot, figure (*c*), shows that the features are not well determined relative to noise in the experimental data.

Both the ELF and AELF difference plots show significant changes (shown in black) in the low-electron-density regions. Fairly large changes might have been expected in these regions owing to the effect of the experimental data, which incorporates in some way the effect of other molecules around the one modelled by the constrained wavefunction. Basis-set effects may also contribute to errors in these regions, but systematic studies of basis-set effects on electron localization functions are lacking at this time.

The differences between the constrained and Hartree–Fock plots are also broadly consistent, but it is clear that the difference plots for the Fermi hole mobility functions show much more structure. For ammonia, all plots show that electron pairs coalesce in a diffuse region midway between the H atoms at the expense of electrons in the lone-pair region. The same build up is seen between the H atoms of urea, and in addition there is a build up of 'electron pairing density' on the CO bond, near the oxygen. This build up is at the expense of density near the C atoms, but opposite to the CO and CH bonds [shown in black in Figs. 1 and 2, part 2(*b*); or green in Figs. 3 and 4, part 2(*b*)].

The broad red–green lines seen in the Fermi-type plots are a consequence of the changes in the shape of the basins of these electron localization functions.

The error plots associated with the electron localization plots are important. They indicate that the changes due to the incorporation of real X-ray data are mostly above the level associated with random noise in the X-ray data. For the ELF and AELF, most of the error tends to be located in low-electron-density regions far from the molecule, whereas, for the Fermi-hole-based functions, the errors tend to be concentrated in shells around the core regions. The errors for ammonia are considerably less than for the other cases.

3. Conclusions

Experimental X-ray wavefunctions have been calculated for crystals of ammonia, urea and alloxan, and a number of electron localization function plots have been exhibited for each, with associated error plots. A number of interesting results were obtained:

The ELF, approximate ELF (AELF) and approximate Fermi hole mobility function (AFHMF) present visually very similar information with regard to electron-shell structure, although the ELF appears to distinguish lone pairs much better than the others. It appears, therefore, that the electron gas reference point shared by these methods is important when it comes to distinguishing electron localization information.

The AELF introduces a number of undesirable artifacts relative to the true ELF: namely, a more compact shell structure and a splitting of electron-pair density within bonds.

The effect seems pathological for hydrogen bonds. These findings confirm earlier results by Tsirelson & Stash (2002).

Of all the electron localization functions, the Fermi hole mobility function (FHMF) seems to provide a rather poor means of distinguishing electron-pair regions relative to other plots. The core-electron structure for H atoms is entirely missing. In addition, the long-range behaviour of the FHMF makes it slightly more difficult to plot and interpret compared with the other electron localization functions. However, the shape of this function does qualitatively support Luken's arguments (Luken, 1990) that the FHMF can be interpreted as an energy surface for electron transfer.

The errors in the ELF and AELF plots owing to random noise in the experimental data were largest in regions of low electron density. Owing to the unpredictability of these errors, we recommend that error plots of the electron localization functions should always be made.

The Australian Research Council is acknowledged for funding. Discussions with Bill Luken are acknowledged.

References

Bader, R. F. W. (1990). *Atoms in Molecules: a Quantum Theory.* Oxford University Press.

Bader, R. F. W. & Stephens, M. E. (1975). *J. Am. Chem. Soc.* **97**, 7391.

Becke, A. D. & Edgecombe, K. (1990). *J. Chem. Phys.* **92**, 5397–5403.

Boese, R., Niederprüm, N., Bläser, D., Maulitz, A., Antipin, M. & Mallinson, P. R. (1997). *J. Phys. Chem.* B**101**, 5794–5799.

Bytheway, I., Grimwood, D. J., Figgis, B. N., Chandler, G. S. & Jayatilaka, D. (2002). *Acta Cryst.* A**58**, 244–251.

Dunning, T. H. Jr (1970). *J. Chem. Phys.* **53**, 2823–2833.

Figgis, B. N., Sobolev, A. N., Young, D. M., Schultz, A. J. & Reynolds, P. A. (1998). *J. Am. Chem. Soc.* **120**, 8715–8723.

Grimwood, D. J., Bytheway, I. & Jayatilaka, D. (2003). *J. Comput. Chem.* **24**, 470–483.

Grimwood, D. J. & Jayatilaka, D. (2001). *Acta Cryst.* A**57**, 87–100.

Hohenberg, P. & Kohn, W. (1964). *Phys. Rev. B*, **136**, 864–871.

Jayatilaka, D. (1998). *Phys. Rev. Lett.* **80**, 798–801.

Jayatilaka, D. & Grimwood, D. J. (2001). *Acta Cryst.* A**57**, 76–86.

Kohout, M., Wagner, F. R. & Grin, Y. (2002). *Theor. Chem. Acc.* **108**, 150–156.

Krishnan, R., Binkley, J. S., Seeger, R. & Pople, J. A. (1980). *J. Chem. Phys.* **72**, 650–654.

Luken, W. L. (1982). *Int. J. Quantum Chem.* **22**, 889.

Luken, W. L. (1990). *Properties of the Fermi Hole and Electronic Localization*, Vol. 2, pp. 287–320. Berlin: Springer Verlag.

Luken, W. L. & Beratan, D. N. (1982). *Theor. Chim. Acta*, **61**, 265.

Luken, W. L. & Culberson, J. C. (1982). *Int. J. Quantum Chem. Symp.* **16**, 265–276.

Luken, W. L. & Culberson, J. C. (1984). *Theor. Chim. Acta*, **66**, 279.

Savin, A., Becke, A. D., Flad, J., Nesper, R., Preuss, H. & von Schnering, H. G. (1991). *Angew. Chem. Int. Ed. Engl.* **30**, 409–412.

Schmider, H., Smith, V. H. & Weyrich, W. (1992). *J. Chem. Phys.* **96**, 8986–8994.

Silvi, B. & Savin, A. (1994). *Nature (London)*, **371**, 683–686.

Swaminathan, S., Craven, B. M. & McMullan, R. K. (1984). *Acta Cryst.* B**40**, 300–306.

Swaminathan, S., Craven, B. M. & McMullan, R. K. (1985). *Acta Cryst.* B**41**, 113–122.

Swaminathan, S., Craven, B. M., Spackman, M. A. & Stewart, R. F. (1984). *Acta Cryst.* B**40**, 398–404.

Tsirelson, V. & Stash, A. (2002). *Chem. Phys. Lett.* **351**, 142–148.

Yang, W., Parr, R. G. & Lee, C. (1986). *Phys. Rev. A*, **34**, 4586–4590.

Zhao, Q., Morrison, R. C. & Parr, R. G. (1994). *Phys. Rev. A*, **50**, 2138–2142.

Zhao, Q. & Parr, R. G. (1993). *J. Chem. Phys.* **98**, 543–548.